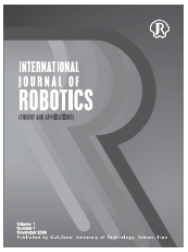

INTERNATIONAL JOURNAL OF ROBOTICS
(THEORY AND APPLICATIONS)
E-mail: IJR@kntu.ac.ir

A Novel Multimode Mobile Robot with Adaptable Wheel Geometry for Maneuverability Improvement

A. Mardani[a], S. Ebrahimi[b,*]

[a] PhD Student, Mechanical Engineering Department, Yazd University, Yazd, Iran.

[b] Associate Professor, Mechanical Engineering Department, Yazd University, Yazd, Iran.

ARTICLE INFO

Article history:

Received: June 3, 2016.
Received in revised form: November 17, 2016.
Accepted: November 20, 2016.

Keywords:

Adaptable Wheel Geometry
Multimode Mobile Robot
Maneuverability
Kinematic Analysis

ABSTRACT

In this paper, an innovative mobile platform is presented which is equipped by three new wheels. The core of the new idea is to establish a new design of rigid circular structure which can be implemented as a wheel by variable radius. The structure of wheel includes a circular pattern of a simple two-link mechanism assembled to obtain a wheel shape. Each wheel has two degrees of freedom. The first is to rotate wheel axis and the second is to change the wheel radius. As the first step, after definition of the new model, its spatial kinematics and constraints will be formulated. The well-known Newton-Raphson algorithm is implemented to find the current response of the kinematic model. A semi-dynamic formulation is further utilized to find the torque of motors for adapting the required wheel radius for maneuverability improvement on rough surfaces. The principles of virtual work will be used to extract the torque values numerically. The ability of the proposed robot for performing the required tasks will finally be checked by some simulations.

1. Introduction

In real applications of mobile robots, improvement of the maneuverability on rough surfaces is a challenging task. A great deal of difficulties arising in this topic can effectively be solved by implementation of a proper and innovative mechanical design. Even a little innovation in this regard may effectively promote the navigation capability and mechanical response of mobile robots. Substantial amount of design efforts have been conducted in this topic to solve different issues including surface disturbance eliminations [1], enhancement of dynamical stability [2-4], reducing number of actuators, weight and the total cost [5-6], increasing the ability of obstacle climbing [7-9], promoting the way of connection between manipulators and the main mobile platform [10], combining the platform and manipulator [1, 11], special design of a mobile platform for certain mission [12-14], generalization of a mobile robot to overcome rough surfaces and trouble conditions [15-16], and reducing or increasing flexibility of platform according to the objective of missions [7]. In the mobile robotics field, a wide range of such novel designs can be classified in the multimode mobile platforms. Wheeled mobile platforms, having almost simple design, fail in a wide range of mission conditions. The primary ideas to promote the performance of mobile manipulators are to increase the number of wheels [17-18] or promotion of the suspension system. These efforts lead to the enhancement of maneuverability and increase of the margin of dynamic stability.

*Corresponding author address: Yazd University, Safayieh, Yazd, Iran.
Tel.: +983531232621; fax: +9835382112781, E-mail address: ebrahimi@yazd.ac.ir.

To promote the ability of obstacle overcoming, a special category of multimode mobile manipulators has been developed by combining the leg and wheel structures [19-20]. Connecting a wheel to the end point of the artificial legs [21-26] or implementing a pattern of wheels [27] leads to the more capable mobile platforms. These efforts focus on the improvement of locomotion ability but the exact controlling of a point of the robot body has been almost missed.

A new design satisfying the locomotion objectives besides controlling a point on the robot body has been investigated in some researches combining locomotion and manipulation as a simplified platform in 2D. However, 3D locomotion and manipulation can be satisfied simultaneously by a novel idea. Therefore, in this paper, a novel idea is proposed by focusing on wheels structure, rather than wheels pattern, to adapt the wheel geometry by changing radius. The new platform is a pattern of simple mechanism connected by means of bended revolute joints to approximate wheel shape. This mechanism is driven by means of a motor to shape the mobile robot wheel. Independent changing of the wheel radius leads to some new advantages for a three-wheeled platform, which allows manipulating a point of the robot body on a certain trajectory. It leads to have a combined platform which can be a multimode structure moving and manipulating as a unique system on rough surfaces.

By some additive instruments like accelerometers installed on each wheel axis, the condition of disturbance elimination will be provided as it has already been done in [1] for 2D. Another advantage will emerge when the objective of mechanical structure is whirling. As the main difference between the newly developed and old structures, the whirling motion can also be obtained by setting the angular velocity of the wheel axis on a constant value and adjusting the wheel radius. In the case of passing over an obstacle, the mission can simply be followed by increasing the height of the robot body as the result of wheel radius adjustment. As another interesting case, the robot can move on a ramp, while its body keeps a desired orientation. As the first part of the present research, the new system will be recognized to be obvious as well as possible. Kinematic parameters, 3D kinematic equations and mathematical definition of the desired path will be presented, respectively; Then, the kinematic constraints will be introduced.

The Newton-Raphson algorithm is used to solve nonlinear system of kinematic equations. Dynamics will be further considered to obtain the torques of additive adjustment motors in each wheel in the presence of gravity forces. The simulations and derivation of equations will be done based on the assumptions such as sticking condition, lumped mass in CG, ignoring centrifugal forces and moving on rough surface.

2. Concept Embodiment

The goal of this section is to define the new platform which includes a mobile robot with three adjustable wheels. The main idea of the new platform is to obtain the ability of adjusting radius of wheels. The key idea of the new platform design is to add a transformable serial pattern of cross mechanisms to the axis of motor of the wheels instead of common circular wheels. Figure (1–a) shows a part which connects the new wheel to the motors. As it can be illustrated, the connection part is a rigid body connected to motors from one side. Other side of the connection part is equipped with prismatic joint. The prismatic joint is a groove in Fig. 1-a. The cross in Fig. 1-b has two links. One of them is restricted by means of a revolute joint, while the other is restricted by means of a prismatic joint. The angle between two links is adjusted by means of the motor which is located in a position shown in Fig. 1-b. a closed-loop serial pattern of the crosses is illustrated in Fig. 1-d. This serial pattern is connected to the cross mechanism mentioned in Fig. 1-b. The closed-loop mechanism is connected to the wheel axis by small pieces which are shown on the right side of the cross linkage in Fig. 1-b. It can be seen in Fig. 1-d that when the motor rotates, the closed-loop mechanism rotates as a wheel. On the other hand, when the restricted cross in Fig. 1-b is driven by means of the adjustment motor, the close-loop mechanism radius is changed. Because the shape of the close-loop mechanism is not a complete wheel, some additive rubbers have to be added as Fig. 1-e illustrates. The effect of rubbers on wheel performance is to complete the circular shape of the wheel and to soften the collision process with the surface. Finally, three complete assembled wheels will be installed on a body as a three-wheeled mobile robot as illustrated in Fig. 1-f.

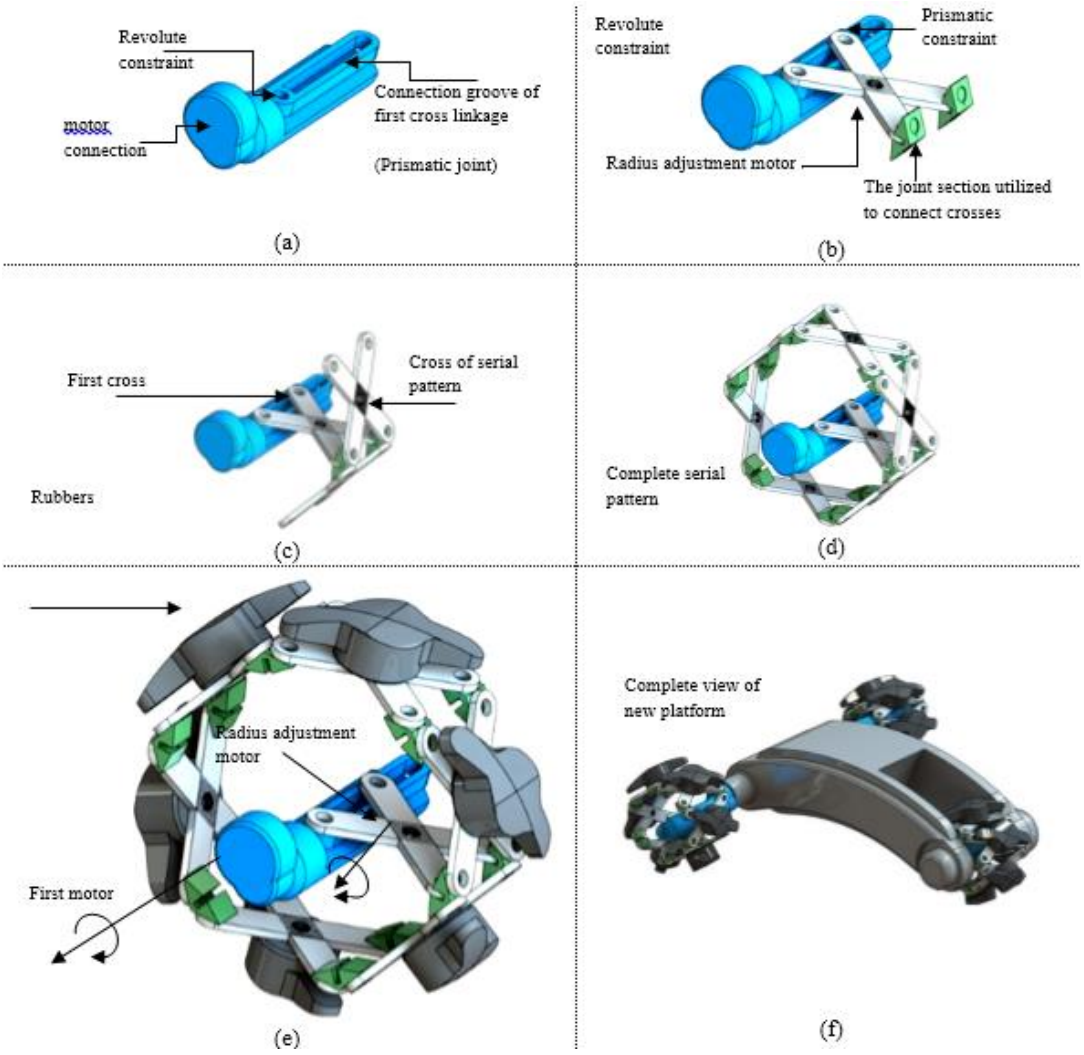

Fig. 1. Assembling process of the new proposed platform

As it was expressed previously, the main idea is to design a rigid and transformable wheel in order to improve the maneuverability on rough surfaces. Figures 2 and 3 show the process of radius adjustment and the complete mobile robot structure with adaptable wheel geometry, respectively.

.

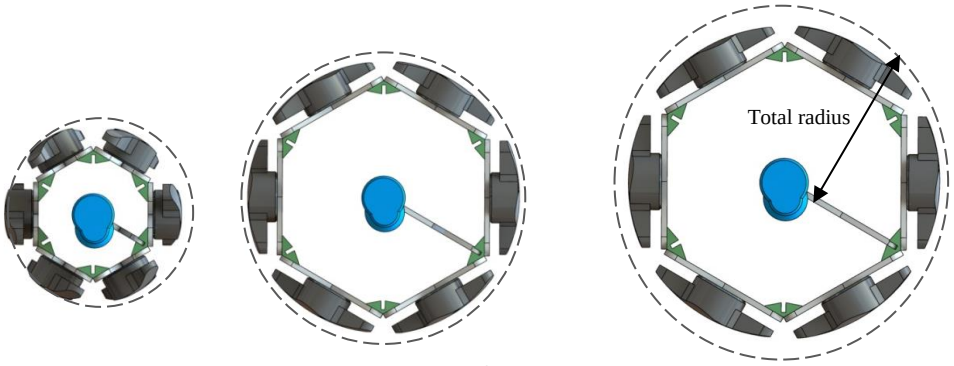

Fig. 2. The process of radius adjustment

Fig. 3. The complete mobile robot structure with adaptable wheel geometry

3. Principle Properties

The main body of the new platform has six degrees of freedom, the same as other mobile robots. Three degrees of freedom including height of CG with respect to the surface, pitch angle and roll angle of the robot body are restricted by wheel radius adjustment. It means that the adjustment motors affect these DOFs. The constraints which control these DOFs as well as the yaw angle of the robot body are holonomic constraints. Two other constraints for controlling x and y positions are non-holonomic. Simple mobile robots only have two non-holonomic constraints (position x and y on the flat surface) and one holonomic constraint (the yaw angle). The majority of these mobile robots cannot control the height, roll angle and pitch angle. Indeed, the adjustable radius of each wheel adds an additive DOF to mobile platform. So, new mobile platform is equipped by three additive DOFs. The final objective is to control roll, pitch and height of the body besides other surface navigation DOFs (yaw angle, x and y positions) simultaneously, by means of six control commands.

A crucial conceptual question which may arise in developing the new platform is that how the signals of the adjustment motors can be conveyed from the robot body to the rotating wheel. This point should be explained to avoid any wire cut-off in one complete rotation of the wheel. The wire cut-off is probable if a side of the wire is fixed in the control and power box and the other side of the wire is connected to the adjustment motor located on a rotating wheel. To solve this issue, an additional part is proposed in appendix A.

4. Kinematics of the New Model

The kinematics of the new structure can be shortened as a conceptual problem. According to Fig. 4, the problem is to find angle θ_i for the desired orientation and position of the CG. Parameter θ_i is the angle of adjustment motor of the i^{th} wheel. Figure 4 shows some geometric and kinematic parameters. Parameter$w$ is the length of leg of each cross linkage determined in Fig. 4. Parameters $2L_x$ and $2L_y$ are the length and width of the robot body, respectively.

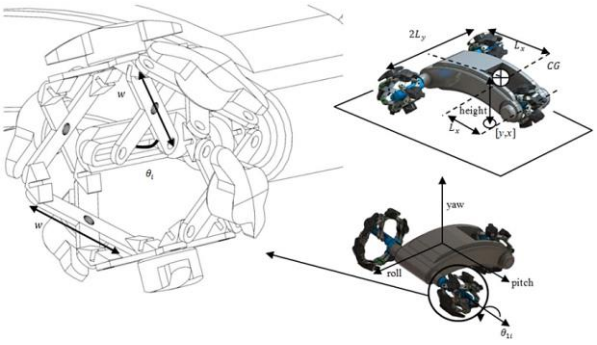

Fig. 4. Geometric and kinematic parameters of body

Other important kinematic parameters are defined in Fig. 5. Parameter β_i is the angle between the axis Y of the wheel coordinate system and the line connecting the wheel center and the contact point of the wheel with the surface. Parameters $R_{ru,i}$, $R_{ch,i}$ and $R_{T,i} = R_{ru,i} + R_{ch,i}$ are the rubber height, the close-loop pattern radius and the total radius of wheel i, respectively. The rubber height $R_{ru,i}$ is constant.

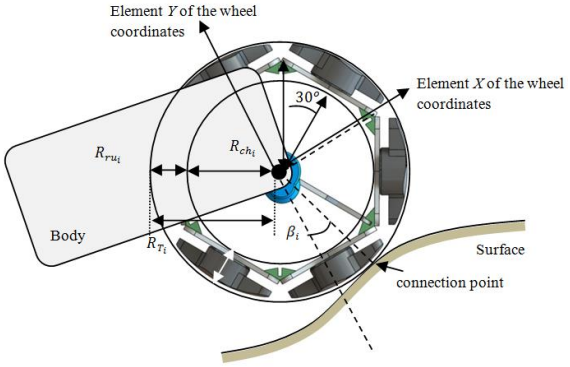

Fig. 5. Geometric and kinematic parameters of the wheel

The close-loop pattern radius is obtained from

$$R_{ch,i}=w\cos(\theta_i/2)\cos(\pi/6) \quad (1)$$

Let the surface equation be denoted with respect to the fixed coordinate as

$$Z=f(x,y) \quad (2)$$

After determination of the kinematic parameters, required coordinate systems are defined in Fig. 6. The first coordinate system $X_0Y_0Z_0$ denotes the global coordinate frame. The reference coordinate system of the robot body attached at CG is denoted as $X_{CG}Y_{CG}Z_{CG}$. The point where the i^{th} wheel connects to the main body is the origin of the coordinate system $X_{1i}Y_{1i}Z_{1i}$.

The coordinate frame attached to the i^{th} wheel at contact point with the surface is denoted as $X_{3i}Y_{3i}Z_{3i}$. Finally, the coordinate system $X_{si}Y_{si}Z_{si}$ is attached to the surface at contact point in a way that its Y_{si} direction is perpendicular to the surface. The Y component of the surface coordinate frame $X_{si}Y_{si}Z_{si}$ is aligned with the normal vector to the surface, which can be expressed as

$$\mathbf{N}(x,y)=[-\frac{\partial f(x,y)}{\partial x},-\frac{\partial f(x,y)}{\partial y},1]^{\mathrm{T}}$$
$$\mathbf{n}=\frac{\mathbf{N}(x,y)}{\|\mathbf{N}(x,y)\|} \quad (3)$$

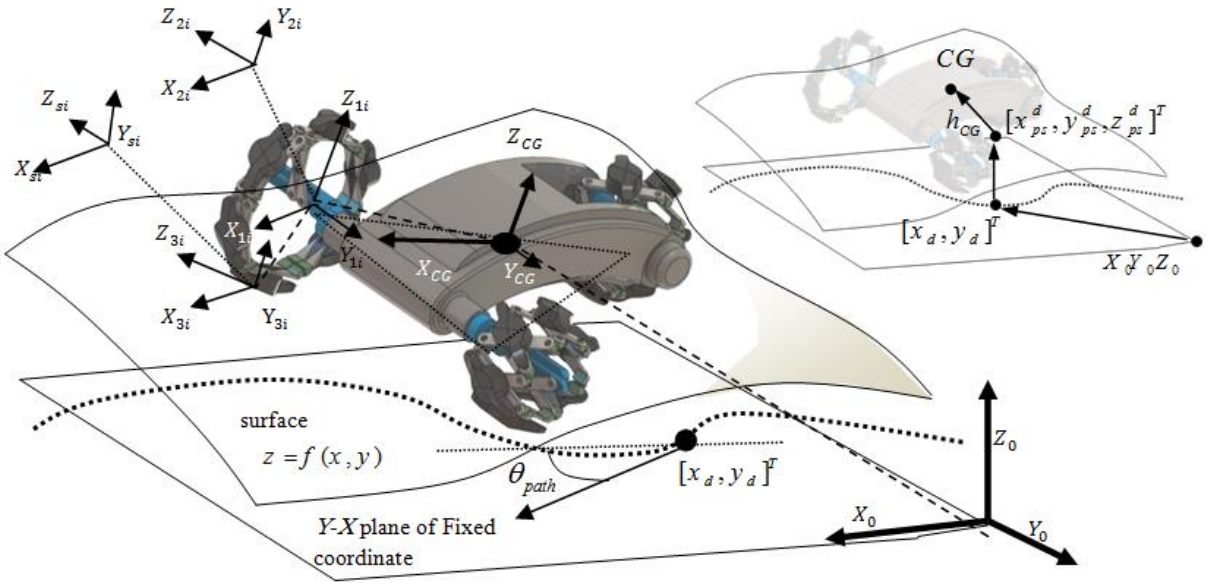

Fig. 6. Coordinate systems of the kinematic problem

where $\mathbf{n}$ denotes the unit normal vector expressed in the global coordinate system $X_0Y_0Z_0$. The homogenous transformation matrices [28] between the body reference and fixed coordinate frames are determined by successive translations and rotations as

$$\mathbf{T}^0_{CG} = \mathbf{T}_{pos}\mathbf{T}_{y,\theta_{yd}}\mathbf{T}_{x,\theta_{xd}}\mathbf{T}_{z,\theta_{zd}}$$

$$\mathbf{T}^0_{CG}=\begin{bmatrix}\mathbf{R}^0_{CG} & \mathbf{d}^0_{CG}\\ \mathbf{0} & 1\end{bmatrix}$$

$$\mathbf{T}_{pos}=\begin{bmatrix}1&0&0&x^d_{CG}\\0&1&0&y^d_{CG}\\0&0&1&z^d_{CG}\\0&0&0&1\end{bmatrix} \quad (4)$$

(4)
$$\mathbf{T}_{y,\theta_{yd}}=\begin{bmatrix}\cos(\theta_{yd})&0&\sin(\theta_{yd})&0\\0&1&0&0\\-\sin(\theta_{yd})&0&\cos(\theta_{yd})&0\\0&0&0&1\end{bmatrix}$$

$$\mathbf{T}_{x,\theta_{xd}} = \begin{bmatrix} 1 & 0 & 0 & 0 \\ 0 & \cos(\theta_{xd}) & -\sin(\theta_{xd}) & 0 \\ 0 & \sin(\theta_{xd}) & \cos(\theta_{xd}) & 0 \\ 0 & 0 & 0 & 1 \end{bmatrix}$$

$$\mathbf{T}_{z,\theta_{zd}} = \begin{bmatrix} \cos(\theta_{zd}) & -\sin(\theta_{zd}) & 0 & 0 \\ \sin(\theta_{zd}) & \cos(\theta_{zd}) & 0 & 0 \\ 0 & 0 & 1 & 0 \\ 0 & 0 & 0 & 1 \end{bmatrix} \quad (4)$$

Where $\boldsymbol{T}_{y,\theta_{yd}}$, $\boldsymbol{T}_{x,\theta_{xd}}$ and $\boldsymbol{T}_{z,\theta_{zd}}$ denote the rotation matrices resulting from the rotation about the fixed axes *Y*, *X* and *Z*, with angles θ_{yd} , θ_{xd} and θ_{zd} , respectively. Furthermore, let the desired CG position, $[x^d_{CG}, y^d_{CG}, y^d_{CG}]^{\mathrm{T}}$, be determined in terms of $[x_d, y_d]^{\mathrm{T}}$ which define coordinates of a point on the desired path in the current time simulation interval. To do so, we first consider a point with coordinates $[x^d_{ps}, y^d_{ps}, z^d_{ps}]^{\mathrm{T}}$ on the 3D surface which is located exactly above that point of the desired path. Therefore, one can write

$$[x^d_{ps}, y^d_{ps}, z^d_{ps}]^{\mathrm{T}} = [x_d, y_d, f(x_d, y_d)]^{\mathrm{T}} \quad (5)$$

We further define the distance between this point defined by Eq. (5) and the CG position by h_{CG} which is indeed in direction of the normal vector $\mathbf{N}$ of Eq. (3). The desired CG position can now be calculated as

$$[x^d_{CG}, y^d_{CG}, y^d_{CG}]^{\mathrm{T}} = h_{CG}\mathbf{n}(x^d_{ps}, y^d_{ps}) + [x^d_{ps}, y^d_{ps}, z^d_{ps}]^{\mathrm{T}} \quad (6)$$

In order to specifically define the coordinate frames $X_{3i}Y_{3i}Z_{3i}$ at contact points, an index is given to each wheel specifying its relative position with respect to the body reference coordinate frame $X_{CG}Y_{CG}Z_{CG}$. Therefore, the indices *fr* , *fl* and *r* are considered to denote the front right, front left and rear wheels, respectively. The homogenous transformation matrix between the fixed coordinate frame $X_0Y_0Z_0$ and coordinate frame $X_{3i}Y_{3i}Z_{3i}$ for three wheels are determined as

$$\mathbf{T}^0_{3i} = \mathbf{T}^0_{CG}\mathbf{T}^{CG}_{1i}\mathbf{T}^{1i}_{2i}\mathbf{T}^{2i}_{\beta}\mathbf{T}^{\beta}_{3i} = \begin{bmatrix} \mathbf{R}^0_{3i} & \mathbf{d}^0_{3i} \\ \mathbf{0} & 1 \end{bmatrix}, \ (i = fr, fl, r) \quad (7)$$

The first matrix on the right hand side of the above equations was previously defined in Eq. (4). The homogenous transformation matrices $\mathbf{T}^{CG}_{1i}(i = fr, fl, r)$ specify transformation between frames $X_{CG}Y_{CG}Z_{CG}$ and $X_{1i}Y_{1i}Z_{1i}$ which are defined as

$$\mathbf{T}^{CG}_{1fr} = \begin{bmatrix} \mathbf{I}_{3\times3} & \begin{bmatrix} L_x, -L_y, 0 \end{bmatrix}^T \\ \mathbf{0}_{1\times3} & 1 \end{bmatrix}$$

$$\mathbf{T}^{CG}_{1fl} = \begin{bmatrix} \mathbf{I}_{3\times3} & \begin{bmatrix} L_x, L_y, 0 \end{bmatrix}^T \\ \mathbf{0}_{1\times3} & 1 \end{bmatrix} \quad (8)$$

$$\mathbf{T}^{CG}_{1r} = \begin{bmatrix} \mathbf{I}_{3\times3} & \begin{bmatrix} -L_x, 0, 0 \end{bmatrix}^T \\ \mathbf{0}_{1\times3} & 1 \end{bmatrix}$$

In order to align the *Z* axis of the coordinate frame $X_{1i}Y_{1i}Z_{1i}$ with the direction of the wheel axis, a rotation of 90° about its *X* axis is performed to obtain the coordinate frame $X_{2i}Y_{2i}Z_{2i}$. This results in the transformation matrices $\boldsymbol{T}^{1i}_{2i}(i = fr, fl, r)$ as

$$\mathbf{T}^{1fr}_{2fr} = \mathbf{T}^{1r}_{2r} = \begin{bmatrix} 1 & 0 & 0 & 0 \\ 0 & 0 & -1 & 0 \\ 0 & 1 & 0 & 0 \\ 0 & 0 & 0 & 1 \end{bmatrix}$$

$$\mathbf{T}^{1fl}_{2fl} = \begin{bmatrix} 1 & 0 & 0 & 0 \\ 0 & 0 & 1 & 0 \\ 0 & -1 & 0 & 0 \\ 0 & 0 & 0 & 1 \end{bmatrix} \quad (9)$$

Furthermore, the homogeneous transformation matrices $\mathbf{T}^{2i}_{\beta}(i = fr, fl, r)$ align the *Y* axis of the current frame with the line connecting the wheel center and the contact point of the wheel $X_{2i}Y_{2i}Z_{2i}$ and $X_{3i}Y_{3i}Z_{3i}$, and are defined as

$$\mathbf{T}^{2i}_{\beta} = \begin{bmatrix} \cos(\beta_i) & -\sin(\beta_i) & 0 & 0 \\ \sin(\beta_i) & \cos(\beta_i) & 0 & 0 \\ 0 & 0 & 1 & 0 \\ 0 & 0 & 0 & 1 \end{bmatrix} \quad (10)$$

$(i = fr, fl, r)$

Finally, the transformation matrices $\mathbf{T}^{\beta}_{3i}(i = fr, fl, r)$ perform required translations to reach the origin of the frame $X_{3i}Y_{3i}Z_{3i}$ at contact points

$$\mathbf{T}_{3fr}^{\beta}=\begin{bmatrix}\mathbf{I}_{3\times3} & \left[0,-R_{T,fr},0\right]^{\mathrm{T}}\\ \mathbf{0}_{1\times3} & 1\end{bmatrix}$$
$$\mathbf{T}_{3r}^{\beta}=\begin{bmatrix}\mathbf{I}_{3\times3} & \left[0,-R_{T,r},0\right]^{\mathrm{T}}\\ \mathbf{0}_{1\times3} & 1\end{bmatrix} \qquad (11)$$
$$\mathbf{T}_{3fl}^{\beta}=\begin{bmatrix}\mathbf{I}_{3\times3} & \left[0,R_{T,fl},0\right]^{\mathrm{T}}\\ \mathbf{0}_{1\times3} & 1\end{bmatrix}$$

Where $R_{T,fr}$, $R_{T,fl}$ and $R_{T,r}$ denote the front-right, front-left and rear wheel radiuses, respectively, which have been recently introduced in Section 4. As stated before in Section 3, six control commands are supposed to control roll, pitch and yaw angles, x and y positions of the desired path, and height of the body. These commands are summarized in a vector as $[\theta_{xd},\theta_{yd},\theta_{zd},h_{CG},x_d,y_d]^{\mathrm{T}}$.

5. Kinematic Constraints

The constraints can be classified into two main categories, namely contact point position constraints and contact surface constraints. All points of the wheel which can be in contact with a surface are assumed to locate on a rim. This assumption shrinks a 3D model of the wheel to a simplified one. It means that the thickness of the wheel can be neglected. In this model, it is assumed that the wheel is without thickness capable of adjusting its radius. This assumption provides simpler mathematical expression of the wheel in the 3D space. So, the contact point of the wheel can simply be found through this assumption. For algorithms simulating contact the readers are referred to, e.g. [29, 30].

The six control commands that robot body has to follow were determined previously. The constraints which will be explained have to take zero value. The position constraints are defined as

$$C_i=\mathbf{d}_{3i}^{0}(3)-f(x,y),\quad (i=fr,fl,r)$$
$$x=\mathbf{d}_{3i}^{0}(1),\quad y=\mathbf{d}_{3i}^{0}(2) \qquad (12)$$

This equation implies that the Z components of the contact point of each wheel denoted by $\mathbf{d}_{3i}^{0}(3)$ (introduced in Eq. (7)) and its associated point of the surface are equal. For the contact surface constraints, it is required that the first component of the normal vector $\mathbf{N}(x,y)$ of Eq. (3) at contact points, when represented in the coordinate system $X_{3i}Y_{3i}Z_{3i}$, vanishes. This condition guarantees to obtain a feasible contact between each wheel and surface. The normal vector $\mathbf{N}(x,y)$ in the coordinate system $X_{3i}Y_{3i}Z_{3i}$, can be represented as, see Fig. (7),

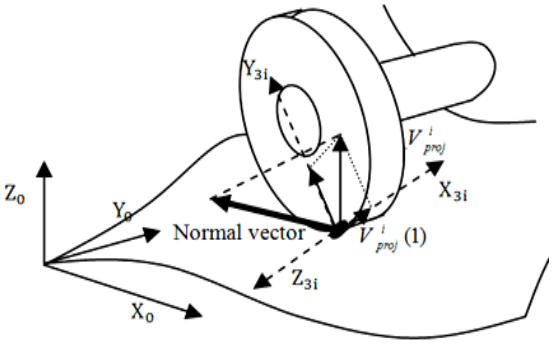

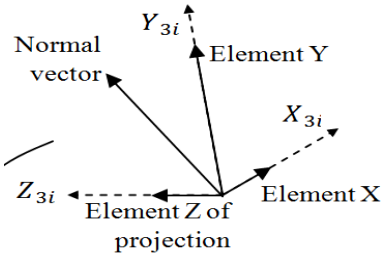

Fig. 7. Representation of the normal vector in the coordinate system $X_{3i}Y_{3i}Z_{3i}$

$$\mathbf{V}_{proj}^{i}=(\mathbf{R}_{3i}^{0})^{\mathrm{T}}\mathbf{N}(x,y)$$
$$x=\mathbf{d}_{3i}^{0}(1),\quad y=\mathbf{d}_{3i}^{0}(2) \qquad (13)$$
$$(i=fr,fl,r)$$

Therefore, the contact surface constraints can be written as

$$CC_i=[1\ \ 0\ \ 0]\,\mathbf{V}_{proj}^{i}=\mathbf{V}_{proj}^{i}(1) \qquad (14)$$
$$(i=fr,fl,r)$$

These constraints can be combined with constraint equations of Eqs. (12) to obtain the vector of kinematic constraints as

$$\mathbf{C} = [C_{fr}, C_{fl}, C_r, CC_{fr}, CC_{fl}, CC_r]^{\mathrm{T}} = \mathbf{0} \qquad (15)$$

The Newton-Raphson algorithm [31] is used in this paper for solving the system of nonlinear constraint equations (15) and obtaining the desired solution vector

$$\mathbf{q} = [\beta_{fr}, \beta_{fl}, \beta_r, \theta_{fr}, \theta_{fl}, \theta_r]^{\mathrm{T}} \qquad (16)$$

The constraint Jacobian matrix ***J*** is driven by taking the partial derivatives of **C** with respect to **q** as

$$\mathbf{J} = \frac{\partial \mathbf{C}}{\partial \mathbf{q}} \qquad (17)$$

Prior to simulation, it is desired to choose the numerical values of robot parameters including surface equation (Eq.(2)), x_d and y_d of the desired path equation, h_{CG}, orientation of the robot body $(\theta_{xd}, \theta_{yd}, \theta_{zd})$ and geometric parameters w, L_x, L_y and $R_{ru,i}$. All of these parameters can be defined independently but θ_{zd}. As it can be understood from the previous sections, θ_{zd} is the current rotation angle performed after rotations θ_{xd} and θ_{yd}. This angle is particularly dependent of the desired path for which the following relation holds

$$\frac{dy_d}{dx_d} = \tan(\theta_{path}) \Rightarrow \frac{\dot{y}_d}{\dot{x}_d} = \tan(\theta_{path}) \qquad (18)$$

Where θ_{path}, x_d and y_d are defined in Fig. 6. The angular velocity vector of the desired path denoted by $\boldsymbol{\omega}_{path}$ is then written by taking the derivative of Eq. (18) yielding

$$\boldsymbol{\omega}_{path} = [0, 0, \dot{\theta}_{path}]^{\mathrm{T}} = \left[0, 0, \frac{\ddot{y}_d \dot{x}_d - \ddot{x}_d \dot{y}_d}{\dot{x}_d^{\,2}} \cos^2(\theta_{path})\right]^{\mathrm{T}} \qquad (19)$$

We further define the angular velocity vector of the robot in the body reference coordinate frame $X_{CG}Y_{CG}Z_{CG}$ as $\boldsymbol{\omega}_{robot}^{CG} = \left[\dot{\theta}_{xd}, \dot{\theta}_{yd}, \dot{\theta}_{zd}\right]^{\mathrm{T}}$. It is then transformed into the fixed coordinate system $X_0Y_0Z_0$.The orientation of robot about axis Z is directly defined by the steering command obtained from the path direction in such a way that the robot follows the desired path accurately. Therefore, the Z components of $\boldsymbol{\omega}_{robot}^{0}$ and $\boldsymbol{\omega}_{path}$ have to be the same.

$$\boldsymbol{\omega}_{robot}^{0} = \mathbf{R}_{CG}^{0} \boldsymbol{\omega}_{robot}^{CG} = \mathbf{R}_{CG}^{0} \left[\dot{\theta}_{xd}, \dot{\theta}_{yd}, \dot{\theta}_{zd}\right]^{\mathrm{T}} \qquad (20)$$

The orientation of robot about Z axis is directly defined by the steering command obtained from the path direction in such a way that the robot follows the desired path accurately. Therefore, the Z components of $\boldsymbol{\omega}_{robot}^{0}$ and $\boldsymbol{\omega}_{path}$ have to be the same, yielding

$$\boldsymbol{\omega}_{robot}^{0} = \left[\omega_X, \omega_Y, \omega_Z\right]^{\mathrm{T}} = \left[\omega_X, \omega_Y, \dot{\theta}_{path}\right]^{\mathrm{T}} \qquad (21)$$

Which by using Eq. (20) yields

$$\dot{\theta}_{zd} = \frac{\dot{\theta}_{path} - \mathbf{R}_{CG}^{0}(3,1:2)\left[\dot{\theta}_{xd}, \dot{\theta}_{yd}\right]^{\mathrm{T}}}{\mathbf{R}_{CG}^{0}(3,3)} \qquad (22)$$

Substituting $\dot{\theta}_{path}$ from Eq. (19) into Eq. (22) leads to

$$\dot{\theta}_{zd} = \frac{1}{\mathbf{R}_{CG}^{0}(3,3)} \left(\frac{\dot{y}_d x_d - \dot{x}_d y_d}{x_d^{\,2}} \cos^2(\theta_{path}) - \mathbf{R}_{CG}^{0}(3,1:2)\left[\dot{\theta}_{xd}, \dot{\theta}_{yd}\right]^{\mathrm{T}}\right) \qquad (23)$$

Equation (23) denotes that the required angular velocity about yaw axis of the robot body which satisfies the desired commands ($[\theta_{xd}, \theta_{yd}, \theta_{zd}, h_{CG}, x_d, y_d]^{\mathrm{T}}$) is derived in terms of the parameters of the desired path as well as the rotation matrix of the CG coordinate frame. The iterative Newton-Raphson algorithm is initialized by an estimate for the solution vector **q** and is performed in the following manner till the convergence is achieved

$$d\mathbf{q} = -\mathbf{J}^{-1}\mathbf{C} \Rightarrow \mathbf{q}_{k+1} = (-\mathbf{J}^{-1}\mathbf{C}) + \mathbf{q}_k, \quad \text{error} = \text{norm}(\mathbf{C}) \qquad (24)$$

The computational scheme for the kinematic analysis of the mobile robot moving on a rough surface according to the desired path is shown in Fig. 8. It is maybe important to notice that in this algorithm, the commands vector $[\theta_{xd}, \theta_{yd}, \theta_{zd}, h_{CG}, x_d, y_d]^{\mathrm{T}}_{t=t_i}$ is a function of time and can be updated from the current time (t_i) to the next time (t_{i+1}) by substituting t_{i+1} into the time-based functions which are included in this vector.

6. Calculation of Motor Torques for Wheel Radius Adjustment

In this section, the motor torques required for adjusting the radius of wheels are calculated. For this purpose, there is no need to implement a complete dynamic modeling to find all motor torques. Instead, a static

analysis is presented based on the equilibrium equations and virtual work approach.

In this regard, the effect of gravity on the amount of motor torques is investigated. In the absence of slipping, the contact forces caused by gravity are shown in Fig. 9 and are denoted by $\mathbf{F}_{fr}$, $\mathbf{F}_{fl}$ and $\mathbf{F}_{r}$.

In the first step, the contact forces are obtained from six equilibrium equations which can be written in the global coordinate system as

$$\begin{cases} F_{fl_x} + F_{fr_x} + F_{r_x} = 0 \\ F_{fl_y} + F_{fr_y} + F_{r_y} = 0 \\ F_{fl_z} + F_{fr_z} + F_{r_z} = -mg \\ \boldsymbol{F}_{fr} \times \boldsymbol{V}_{CG}^{fr} + \boldsymbol{F}_{fl} \times \boldsymbol{V}_{CG}^{fl} + \boldsymbol{F}_{r} \times \boldsymbol{V}_{CG}^{r} = \mathbf{0} \end{cases} \quad (25)$$

The vector $\boldsymbol{V}_{CG}^{i}$ $(i = fr, fl, r)$ denotes the vector between the robot body CG and contact point of the i^{th} wheel with surface

$$\boldsymbol{V}_{CG}^{i} = \mathbf{d}_{3i}^{CG} = \mathbf{d}_{3i}^{0} - \mathbf{d}_{CG}^{0}, \quad (i = fr, fl, r) \quad (26)$$

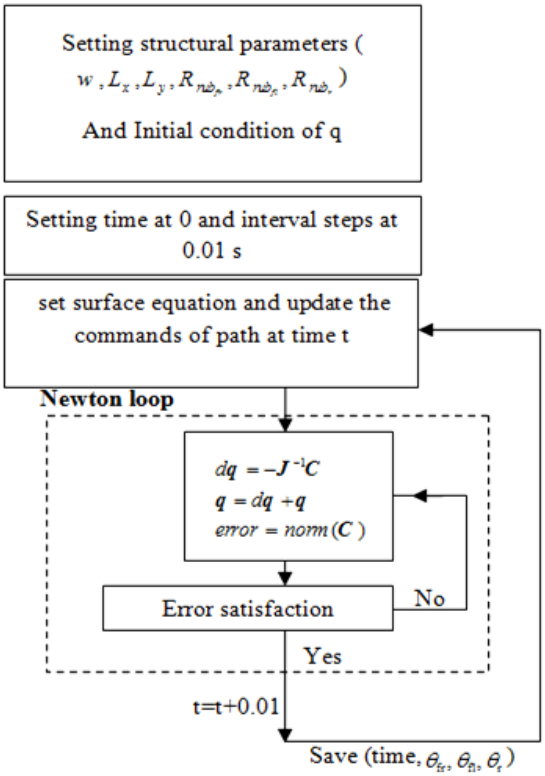

Fig. 8. Flowchart for the kinematic analysis

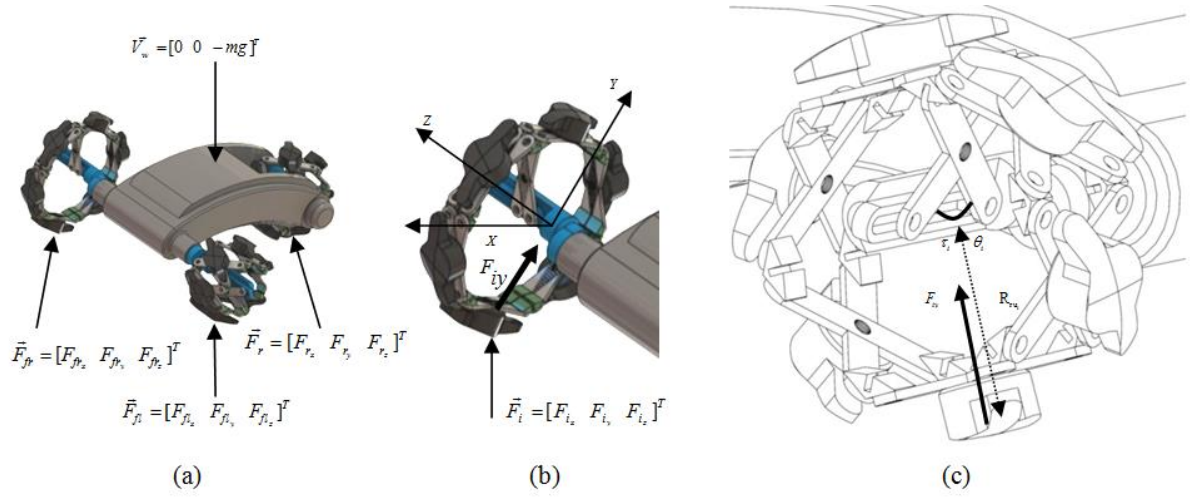

Fig. 9. Contact forces of the wheels at contact points

Each contact force includes three unknown components, resulting in total nine unknowns. Solving this underdetermined system of equations requires imposing some restrictions on the components of contact forces. The first condition is based on the fact that the normal contact forces exerted to the wheels have to be positive for preserving the contact. These normal contact forces can simply be obtained in the surface coordinate system $X_{si}Y_{si}Z_{si}$ from the following relation

$$\mathbf{P}_i = (\mathbf{R}_{3i}^0)^{\mathrm{T}} \left((\mathbf{F}_i . \mathbf{n}_i) \mathbf{n}_i \right), \quad (i = fr, fl, r) \tag{27}$$

This condition means that the Y component of these normal contact forces takes positive value as

$$\mathbf{P}_i(2) \geq 0, \qquad (i = fr, fl, r) \tag{28}$$

The second condition is considered to prevent the wheels to slip on the surface. The non-slip situation is clearly occurred when the friction force between each wheel and the surface does not exceed its maximum value. The magnitude of friction forces can be obtained by

$$f_i = \sqrt{\|\mathbf{F}_i\|^2 - \|\mathbf{P}_i\|^2}, \qquad (i = fr, fl, r) \tag{29}$$

Therefore, the second condition can be presented as

$$f_i \leq \mu_s \|\mathbf{P}_i\|, \qquad (i = fr, fl, r) \tag{30}$$

where μ_s is the coefficient of static friction. For solving the system of equations (25) with constraints (28) and (30), a constrained multiobjective optimization procedure has to be used to obtain the contact forces $\boldsymbol{F}_i$ $(i = fr, fl, r)$ which can finally be transformed from the global coordinate system to the wheel coordinate system as

$$\mathbf{F}_i^{3i} = (\mathbf{R}_{3i}^0)^{\mathrm{T}} \mathbf{F}_i, \ (i = fr, fl, r) \tag{31}$$

The principle of virtual work is then served to find the torques required for maintaining the robot in static equilibrium. These torques are to be applied to keep the wheel in a certain radius. According to the principle of virtual work, the total work of the contact force $\mathbf{F}_i^{3i}$ for changing the wheel radius $dR_{T,i}$ is equal to the work of adjustment motor torque denoted by τ_i for generating $d\theta_i$

$$\mathbf{F}_i^{3i}(2)\ dR_{T,i} = \tau_i d\theta_i, \ (i = fr, fl, r) \tag{32}$$

The relation between $dR_{T,i}$ and $d\theta_i$ can simply be obtained by differentiating Eq. (1), yielding

$$dR_{T,i} = dR_{ch,i} = -0.5w\sin(\frac{\theta_i}{2})\cos(\frac{\pi}{6})d\theta_i, \ (i = fr, fl, r) \tag{33}$$

Substituting Eq. (33) into Eq. (32) results in

$$-0.5\mathbf{F}_i^{3i}(2)w\sin(\theta_i/2)\cos(\pi/6) = \tau_i \quad (i = fr, fl, r) \tag{34}$$

In order to be more conservative, we consider the worst case when the robot moves on a flat surface. In this condition, the contact forces exerted to each wheel are equal to the one-third of the robot weight. Therefore, we replace $\mathbf{F}_i^{3i}(2)$ by $mg/3$ in Eq. (34), leading to the following relation for estimating the motor torques required for wheel radius adjustment

$$\tau_i = \frac{-0.5\, mg\, \mathrm{w}\sin(\theta_i/2)\cos(\pi/6)}{3}, \quad (i = fr, fl, r) \tag{35}$$

7. Concept of sensor implementation

The control process of this new platform is not considered in this study. However, in the forward and inverse kinematic processes during locomotion on the surface, the current position and orientation data of the platform main body have to be detected. In the virtual locomotion, these data can be read from a couple of accelerometers and gyroscopes located in the mass center of the body. The system adjusting the wheels' radius receives the position of the mass center in terms of the absolute position and orientation coordinates.

8. Simulations and Results

The first case study investigated here is the mission of moving the robot on a rough surface while aligning the axis Z_{CG} of its coordinate frame with the axis Z_0 of the fixed coordinate frame by adjusting the angle of radius adjustment motors. In this mission, the robot has to keep its center of gravity in a certain absolute height ($h_{CG} = 0.15\mathrm{m}$) and to follow a prescribed orientation pattern while tracking a desired path (a circle). This is indeed a surface disturbance elimination process which is to be achieved by finding the proper motor torques to impose the required commands $x_d, y_d, h_{CG}, \theta_{xd}, \theta_{yd}, \theta_{zd}$. Table 1 shows the required model specifications and also the required mission commands. The results of this simulation are illustrated in Figs. 10-12. Figure 10 shows 2D and 3D views of tracking a circle on a rough surface with disturbance elimination. The path shown with number 1 is the projection of the required path on the surface. The path labeled with number 2 is the path tracked by the robot body center of gravity. As it is seen, the

algorithm has accomplished the required task successfully. The obtained angular displacements and torques of the radius adjustment motors are provided in Figs. 11 and 12, respectively. According to these figures, the range of angular displacement is between 20 and 170 degree, and the range of torques in the presence of gravity is 1.4 to 4 Nm.

For further validation of the model and evaluating the accuracy of the kinematic analysis, we investigate the difference between the prescribed commands and the obtained results. Figure 13 shows the error of the algorithm in steering the robot with the constant height $h_{CG} = 0.15\,\text{m}$ as well as aligning the axis Z_{CG} of the robot coordinate frame with the axis Z_0 of the fixed coordinate frame. According to this figure, the proposed model can effectively complete the mission with acceptable accuracy.

Table 1. Model specifications

property	Description	value
$x_d, y_d, H_{CG}, \theta_{xd}, \theta_{yd}, \theta_{zd}$	Commands robot has to follow	$x_d = \sin(t), y_d = \cos(t), h_{CG} = 0.15\text{m},$ $\theta_{xd} = 0, \quad \theta_{yd} = 0, \quad \theta_{zd} = \text{will be updated}$
$[w, L_x, L_y, R_{rub_{fr}}, R_{rub_{fl}}, R_{rub_r}]$	Structural properties	$[0.3, 0.6, 0.6, 0.02, 0.02, 0.02]$
$f(x, y)$	Surface equation	$Z = \sin(0.5(x + y))/15$
[start time, interval, end time]	Simulation times	[0s, 0.01s, 5s]
Error	Satisfaction criterion	10^{-5}
μ_s	Coefficient of friction	1(rubber on concrete)
m	Total mass of the robot	10 Kg

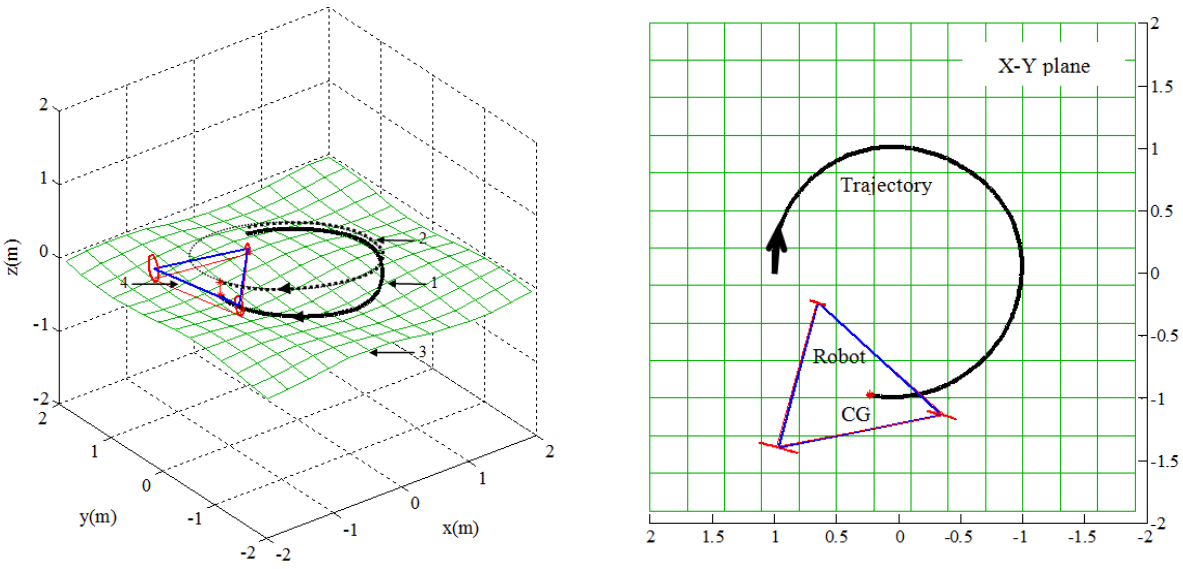

Fig. 10. Mission 1: tracking a circle on rough surface with disturbance elimination (2D and 3D views)

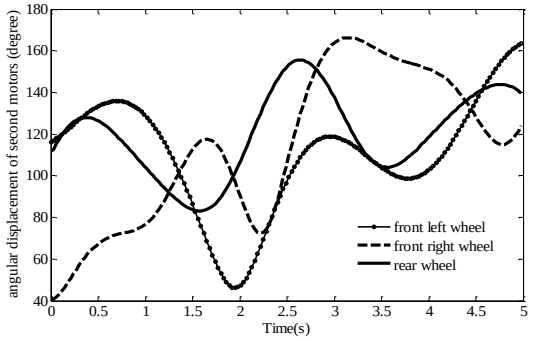

Fig. 11. The angular displacements of the radius adjustment motors in mission 1

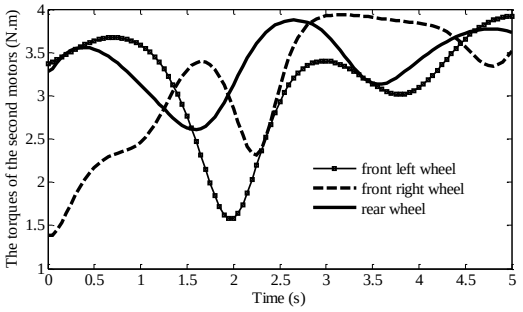

Fig. 12. The torques of the radius adjustment motors in mission 1

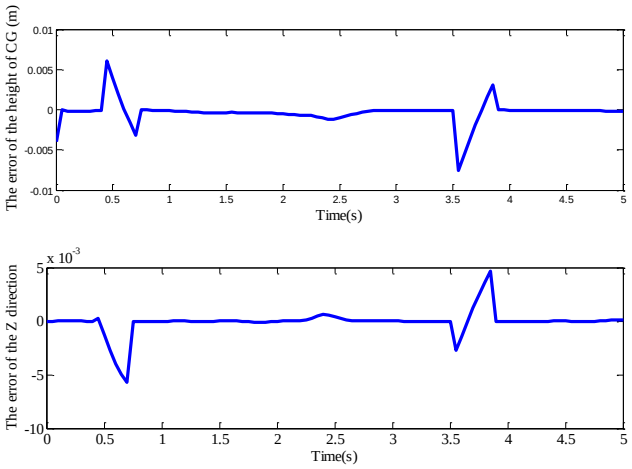

Fig. 13. The error of the kinematic analysis in mission 1

Another important feature of the new multimode mobile robot is the ability to keep the robot body in a horizontal level when the robot is moving on a ramp. A locomotion process on the ramp is conducted to show this ability. According to this simulation, the robot body is forced to be horizontal on a ramp with slope 0.2. Figure 14 shows that the robot has passed this mission successfully. This simulation can be extended to other similar missions. For example, if the robot moves on a ramp with uneven slope, the main body can be horizontal permanently. Table 2 gives the torques and angles of the radius adjustment motors for this mission. As it was investigated at the first simulation, we investigate the difference between the prescribed commands and the obtained results in this mission to validate the model accuracy. Figure 15 confirms that the robot can perform this task successfully.

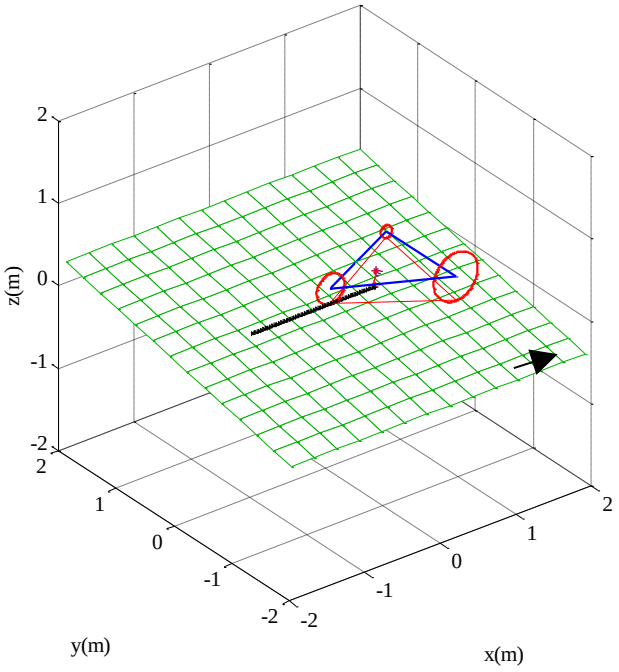

Fig. 14. Mission 2: adjustment of the wheels radius for keeping the robot body in a horizontal level

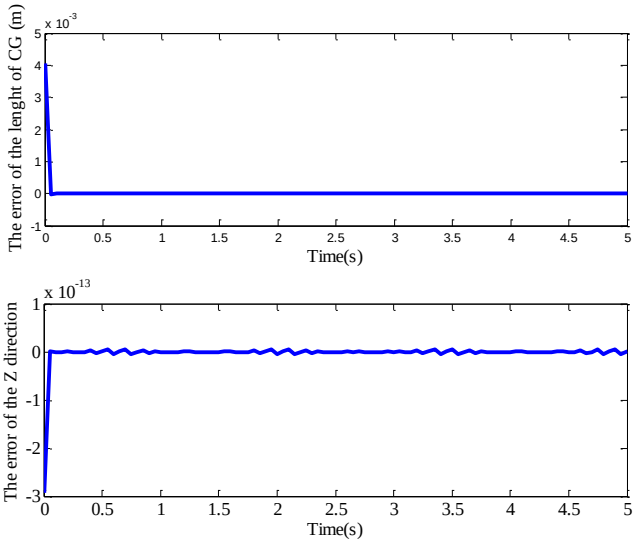

Fig. 15. The error of the kinematic analysis in mission 2

Table. 2. The torques and angles of the radius adjustment motors for mission

motor	torque(Nm)	angle(degree)
rear	3.9	115
front left	1.7	55
front right	3.4	160

9. Conclusion

The new mobile robot mechanical design paradigm presented in this paper was based on compounding of the locomotion and manipulation in the 3D space by means of a rigid adjustable wheel. The article has studied a new rigid adjustable closed-loop mechanism which is implemented as the complete wheel in the mobile platforms. The main objectives of the new platform which were improvement of maneuverability, 6-DOF controlling of the CG and obstacle overcoming have been discussed. Exactly, the maneuverability and 6-DOF locomotion of the CG have been investigated in the simulations. Besides to track the trajectory, the results demonstrate that the new platform is able to eliminate surface disturbance. The additive adjustment motors have been investigated on the torque.

The torque results are in the acceptable range and the required angular displacement of these motors is in the range of 40-170 degrees. So it can be recognized that the body can track each 6-DOF desired command. The future works which will be done to complete the new proposed wheel, are to include the effect of little deformation of the each part of new wheel and to include the effect of friction between joints and links. Also, the other important investigation is to design the complete control loop of the new model including dynamic simulation with uncertainties of the model in the presence of friction and flexibilities, control low in the presence of delays, round of errors, sensor errors and disturbances.

The final future work is to propose interesting motions which new platform can perform.

10. Appendix A.: Additional Part to Avoid Wire Cut-off

To solve the problem of wire cut-off, an additional part is installed on the rotating axis of each wheel as shown in Fig. 16. The additional part sticks to the wheel axis and keeps the rotor of the rotating motors in the hole denoted by number 7. It causes that the disk denoted by number 3 rotates when the wheel starts to rotate. On the other hand, part 2 sticks to the motor body. It means that both motor and part 2 keep their fixed position. Therefore, part 3 can rotate and part 2 keeps the fixed position.

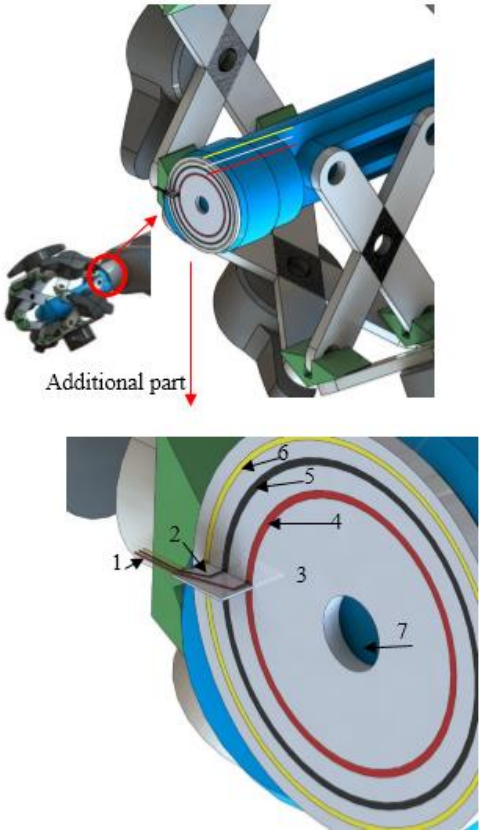

Fig. 16. The additional part to convey power and PWM signal to the adjustment motor

Each servo motor has three signal wires. The red and black wires (which are shown respectively by numbers 4 and 5) conduct the electrical power and the yellow wire (number 6) sends the PWM signal to control the servo motor. Three conductive circular paths are etched on the disk 3 and three conductive brushes convey the signal from the wire denoted by number 1 to the disk 3. In this way, the signals can be conducted from the main body to the rotating wheels without any wire cut-off. All conductive circular paths (numbers 4, 5 and 6) are connected to the servo motor.

References

[1] D. Xu, D. Zhao, J. Yi and X. Tan, Trajectory tracking control of omnidirectional wheeled mobile manipulators: robust neural network-based sliding mode approach. Systems, Man, and Cybernetics, Part B: Cybernetics, IEEE Transactions, Vol. 39(3), (2009), 788-799.

[2] T. B. Lauwers, G. A. Kantor and R. L. Hollis, A dynamically stable single-wheeled mobile robot with inverse mouse-ball drive, Robotics and Automation, ICRA Proceedings IEEE International Conference, (2006), 2884-2889.

[3] S. Ebrahimi, A. Mardani, Dynamic Modeling and Construction of a New Two-Wheeled Mobile Manipulator: Self-balancing and Climbing, International Journal of Robotics, Theory and Applications, Vol. 4(3), (2015), 22-34.

[4] S. Ebrahimi, A. Mardany, Dynamic modeling and construction of a two-wheeled mobile manipulator, part I: Self-balancing, Robotics and Mechatronics (ICROM), (2015), 164-169.

[5] C. Cardeira, J. S. Da Costa, A low cost mobile robot for engineering education, In Industrial Electronics Society, IECON Conference of IEEE, (2005), p. 6.

[6] A. Stengaard, J. Nielsen, M. Skriver, C. Lin and U. Pagh Schultz, Low-cost modular robotic system for neurological rehabilitative training, IEEE International Conference on Industrial Technology (ICIT), (2016), 1585-1591.

[7] A. Mardani, S. Ebrahimi, Dynamic modeling and construction of a two-wheeled mobile manipulator, part II: Modified obstacle climbing. Robotics and Mechatronics (ICROM), (2015), 170-175.

[8] C. S. Casarez, R. S. Fearing, Step climbing cooperation primitives for legged robots with a reversible connection. IEEE International Conference on Robotics and Automation (ICRA), (2016), 3791-3798.

[9] A. S. Boxerbaum, P. Werk, R. D. Quinn and R. Vaidyanathan, Design of an autonomous amphibious robot for surf zone operation: part I mechanical design for multi-mode mobility. Advanced Intelligent Mechatronic Proceedings, IEEE/ASME International Conference, (2005), 1459-1464.

[10] W. McMahan, V. Csencsits, M. Dawson, D. Walker, I. D. Jones and C. D. Rahn, Field trials and testing of the OctArm continuum manipulator. Robotics and Automation. ICRA Proceedings, IEEE International Conference, (2006), 2336-2341.

[11] P. Ben-Tzvi, A. A. Goldenberg and J. W. Zu, Design and analysis of a hybrid mobile robot mechanism with compounded locomotion and manipulation capability, Journal of Mechanical Design, Vol. 130(7), (2008), 072302.

[12] G. C. Haynes, A. Khripin, G. Lynch, J.Amory, Saunders, A. Rizzi and D. Koditschek, Rapid pole climbing with a quadrupedal robot, Robotics and Automation, ICRA'09. IEEE International Conference, (2009), 2767-2772.

[13] F. Xu, J. Shen, J. Hu, and G. Jiang, A rough concrete wall-climbing robot based on grasping claws Mechanical design, analysis and laboratory experiments. International Journal of Advanced Robotic Systems, Vol. 13(5), (2016), 1-10.

[14] M. J. Spenko, G. C. Haynes, J. A. Saunders, M. R. Cutkosky, A. A. Rizzi, R. J. Full and D. E. Koditschek, Biologically inspired climbing with a hexapedal robot, Journal of Field Robotics, Vol. 25(4), (2008), 223-242.

[15] M. P. Mann, Z. Shiller, Dynamic stability of a rocker bogie vehicle: longitudinal motion, Robotics and Automation, ICRA Proceedings of IEEE International Conference, (2005), 861-866.

[16] W. M. Shen, M. Krivokon, H. Chiu, J. Everist, M. Rubenstein and J. Venkatesh, Multimode locomotion via SuperBot reconfigurable robots. Autonomous Robots, Vol. 20(2), (2006), 165-177.

[17] L. Caracciolo, A. Luca and S. Iannitti, tracking control of a four-wheel differentially driven mobile robot, In Robotics and Automation, Proceedings of IEEE International Conference, Vol. 4, (1999), 2632-2638.

[18] T. Estier, Y. Crausaz, B. Merminod, M. Lauria, R. Piguet and R. Siegwart, An innovative space rover with extended climbing abilities, LSA-CONF, (2000), 2000-2003.

[19] H. Adachi, N. Koyachi, T. Arai, A. Shimiza and Y. Nogami, Mechanism and control of a leg-wheel hybrid mobile robot, Intelligent Robots and Systems, Proceedings of IEEE/RSJ International Conference , IROS'99, Vol. 3, (1999), 1792-1797.

[20] H. Tappeiner, S. Skaff, T. Szabo and R. Hollis, Remote haptic feedback from a dynamic running machine, Robotics and Automation, IEEE International Conference, ICRA'09, (2009), 2368-2373.

[21] A. Halme, I. Leppänen, S. Salmi and S. Ylönen, Hybrid locomotion of a wheel-legged machine, Conference on Climbing and Walking Robots, CLAWAR'00, (2000).

[22] B. H. Wilcox, T. Litwin, J. Biesiadecki, J. Matthews, M. Heverly, J. Morrison and B. Cooper, ATHLETE: A cargo handling and manipulation robot for the moon, Journal of Field Robotics, Vol. 24(5), (2007), 421-434.

[23] B. H. Wilcox, ATHLETE: A cargo and habitat transporter for the moon. Aerospace conference, (2009), 1-7.

[24] C. Grand, F. Benamar, F. Plumet and P. Bidaud, Stability and traction optimization of a reconfigurable wheel-legged robot, The International Journal of Robotics Research, Vol. 231(0-11), (2004), 1041-1058.

[25] V. SunSpiral, D. Chavez-Clemente, M. Broxton, L. Keely, P. Mihelich, D. Mittman and C. Collins, FootFall: A ground based operations toolset enabling walking for the ATHLETE rover. Proceedings of AIAA Space Conference, (2008), 1-14.

[26] G. Endo, S. Hirose, Study on roller-walker: multi-mode steering control and self-contained locomotion, Robotics and Automation Proceedings ICRA'00, IEEE International Conference, Vol. 3, (2000), 2808-2814.

[27] M. M. Dalvand, M. Moghadam, Design and modeling of a stair climber smart mobile robot (MSRox), ICAR, Proceedings of the 11th International Conference on Advanced Robotics, (2003), 1062-1067.

[28] M. W. Spong, M. Vidyasagar, Robot dynamics and control, John Wiley & Sons, (2008).

[29] S. Ebrahimi, P. Eberhard, Contact of Planar Flexible Multibody Systems Using a Linear Complementarity Formulation, PAMM Proceedings in Applied Mathematics and Mechanics, Vol. 5(1), (2005), 197-198.

[30] S. Ebrahimi, A Contribution to Computational Contact Procedures in Flexible Multibody Systems. PhD's Thesis, Reihe: Schriften aus dem Institut für Technische und Numerische Mechanik der Universität Stuttgart, Band 8, Shaker Verlag, Germany, (2007).

[31] A. A. Shabana, Computational dynamics, John Wiley & Sons, (2009).

Biography

Arman Mardani is currently a PhD student in the Department of Mechanical Engineering at Yazd University. He received his BSc in Mechanical Engineering in 2012 from Yazd University and his MSc in Mechatronic Engineering in 2014 from Shahrood University. His research interests include robotics, structural design of robots and multibody simulations related to multimode and mobile robots.

Saeed Ebrahimi is currently an associate professor of Mechanical Engineering at Yazd University, Iran. He has received his PhD in Mechanical Engineering from Stuttgart University, Germany, in 2007. He has also completed his postdoctoral fellowship at the Center for Intelligent Machines (CIM), McGill University in 2008. His current research interest includes Dynamic Modelling of Multibody Systems, Robotics, Mechanisms Design and Vibration Analysis of Mechanical Systems.